ACS NANO
Cite This: ACS Nano 2018, 12, 12159−12168
www.acsnano.org

ARTICLE

Exclusive Magnetic Excitation Enabled by Structured Light Illumination in a Nanoscale Mie Resonator

Jinwei Zeng,[†] Mahsa Darvishzadeh-Varcheie,[†] Mohammad Albooyeh,[†] Mohsen Rajaei,[†] Mohammad Kamandi,[†] Mehdi Veysi,[†] Eric O. Potma,*[,‡] Filippo Capolino,*[,†] and H. K. Wickramasinghe*[,†]

[†]Department of Electric Engineering and Computer Science and [‡]Department of Chemistry, University of California Irvine, Irvine, California 92697, United States

Supporting Information

ABSTRACT: **Recent work has shown that optical magnetism, generally considered a challenging light−matter interaction, can be significant at the nanoscale. In particular, the dielectric nanostructures that support magnetic Mie resonances are low-loss and versatile optical magnetic elements that can effectively manipulate the magnetic field of light. However, the narrow magnetic resonance band of dielectric Mie resonators is often overshadowed by the electric response, which prohibits the use of such nanoresonators as efficient magnetic nanoantennas. Here, we design and fabricate a silicon (Si) truncated cone magnetic Mie resonator at visible frequencies and excite the magnetic mode exclusively by a tightly focused azimuthally polarized beam. We use photoinduced force microscopy to experimentally characterize the local electric near-field distribution in the immediate vicinity of the Si truncated cone at the nanoscale and then create an analytical model of such structure that exhibits a matching electric field distribution. We use this model to interpret the PiFM measurement that visualizes the electric near-field profile of the Si truncated cone with a superior signal-to-noise ratio and infer the magnetic response of the Si truncated cone at the beam singularity. Finally, we perform a multipole analysis to quantitatively present the dominance of the magnetic dipole moment contribution compared to other multipole contributions into the total scattered power of the proposed structure. This work demonstrates the excellent efficiency and simplicity of our method of using Si truncated cone structure under APB illumination compared to other approaches to achieve dominant magnetic excitations.**

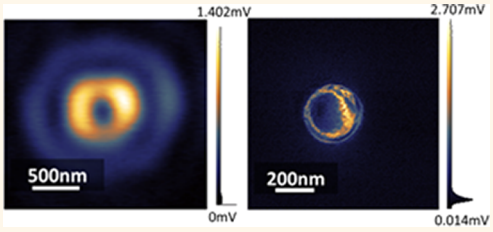

KEYWORDS: *photoinduced force microscopy, magnetic resonance, exclusive magnetic excitation, Mie resonance, structured light, azimuthally polarized beam*

There is a strong interest in the field of nanophotonics to develop methods that can harness optical magnetism of matter at the nanoscale. This is no surprise, as the use and manipulation of optical magnetic transitions offer opportunities in the design of optical devices.[1,2] For example, photomagnetic read/write techniques provide a route toward storing/reading information in single molecules or nanostructures at optical frequencies, promising an enormous increase in capacity.[3−5] In addition, exploiting the fast optical oscillation of light, future optical magnetic imaging can achieve submicron resolution. Furthermore, the use of the photoinduced magnetic force, utilized in the form of optical tweezers, magnetic levitation, force microscopy, *etc.*, opens a window for leveraging the magnetic field of light.[6−10] In short, optical magnetism research is synergetic with modern nanoscience, information technology, and biomedical applications.[11]

Therefore, it is desirable that magnetically responsive materials interact only with the magnetic field of light, so that their magnetic properties can be exclusively employed without significant intervention of the electric response. This is a challenge because, first, most common materials have a rather strong electric response comparing to their magnetic response at optical frequencies;[12] and second, for conventional light, the electric and magnetic fields are coupled through a fixed ratio given by the wave impedance.

Another challenge is nanoscale characterization of optical magnetism. Conventional far-field optical microscopy techniques based on scattering intensity measurements are insufficient for this purpose. Since most natural materials

Received: July 30, 2018
Accepted: December 5, 2018
Published: December 5, 2018

DOI: 10.1021/acsnano.8b05778
ACS Nano 2018, 12, 12159−12168

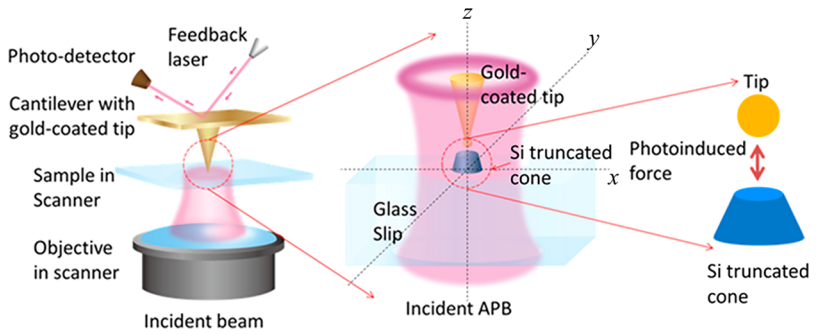

Figure 1. Left, Schematic of the PiFM that is used in our experiment; middle, the magnified region of the gold-plated tip and the sample on the glass slip; right, the model of the interactive gold tip-sample system. The tip and the sample are represented by a gold sphere and a Si truncated cone, respectively.

have a very weak magnetic response at optical frequencies, optical magnetism is usually undetectable.[2,13−15] In addition, optical microscopy is diffraction limited and cannot achieve the subwavelength nanoscale resolution needed to sufficiently resolve the relevant nanostructures.[14,16]

We seek solutions to overcome the discussed challenges. First, to achieve exclusive interaction between the magnetic response of matter and the magnetic field of light, we use an azimuthally symmetric silicon (Si) truncated cone magnetic Mie resonator and incident structured light of an azimuthally polarized beam (APB). The azimuthal polarization of the APB creates a singularity at the beam axis, where the electric field is vanishing and the longitudinal magnetic field is maximized.[17] As a result, along the beam axis and its vicinity, there is a magnetic dominant region where only the magnetic field is significant. The APB will be used as the illumination source to excite the magnetic Mie resonance in the Si truncated cone. Note that both the Si truncated cone and the illuminating APB have azimuthal symmetry and it is important to have the special condition where magnetic field is dominant on the axis.

Second, to characterize nanoscale optical magnetism, we use a near-field probing technique, in particular, photoinduced force microscopy (PiFM). In contrast to optical microscopy that *sees* specimens from far-field probing of the scattered field, the PiFM *feels* specimens directly from the near-field interaction force between a subwavelength probe-tip and the sample surface.[9,18−22] PiFM possesses the merits that are desired for our purpose. Most importantly, force detection enables the measurement of photoinduced electric or magnetic forces which can be related to the corresponding electric or magnetic material properties.[9,17,20,23,24] Furthermore, the photoinduced force exerted on the probe-tip is always local on a subwavelength scale and independent of background scattering photons, in contrast to far-field microscopy.[17,23−25] Therefore, PiFM has a high intrinsic resolution, limited only by the size of the tip, and low background noise.[17,24] Finally, the force is a vector quantity with both amplitude and direction, which provides more information than the detected power in far-field light scattering measurements.[26−28] The instrument used here employs a gold-coated tip, as the probe of the photoinduced electric force in a modified atomic force microscopy (AFM) system.[17,18,24,25,29] The PiFM detects the photoinduced electric force that indicates the local electric field intensity distribution of light near a nanoscale sample, with superior signal-to-noise ratio (SNR) and stability compared to light scattering based techniques such as near-field scanning optical microscopy (NSOM).[17,23,24]

To summarize, in this work we design and fabricate a nano Si truncated cone as the magnetic resonant structure at visible frequencies. Then illuminating the Si truncated cone with a tightly focused APB, we acquire the electric near-field distribution in the vicinity of the top surface of the Si truncated cone by the PiFM. Next, we numerically investigate the proposed structure *via* full wave simulations with excellent matching of the electric near-field distribution to that obtained *via* experimental measurement and use the model to demonstrate the magnetic response described by the normalized local field admittance and magnetic field enhancement at the center of the structure. Finally, we perform a multipole analysis to quantitatively calculate the contribution of the magnetic dipole of the proposed structure to the total scattered power. This result provides the near-field characterization of exclusive magnetic excitation with fidelity and also illustrates the promising applications of the method described in this paper to characterize the electric near-field distribution of nanoscale samples under structured light illumination in general cases.

RESULTS AND DISCUSSION

PiFM Principle. PiFM is the key instrument in this work to characterize the Si truncated cone magnetic resonator under APB illumination. The principle of PiFM has been discussed extensively in previous works.[17,18,23−25,30] In summary, the PiFM employs a conductive tip in an oscillating cantilever as the probe for electric field in an AFM system. When the tip is engaged to a sample surface with external illumination, the tip-apex that resembles a "grain" is polarized as an electric dipole interacting with the image dipole in the sample. Such electric dipole−dipole interaction force constitutes the majority of the photoinduced force, which is often attractive and can be characterized by monitoring the decrease of the cantilever oscillation amplitude.[17,23,25] It is noteworthy that the total force exerted on the tip also includes nonphotoinduced forces, such as van der Waals, chemical, viscous, *etc.*, that contribute to the topography measurement of AFM. The photoinduced force is efficiently separated from the nonphotoinduced force by a multifrequency lock-in mechanism.[17,23,24]

Here we use a commercial PiFM, the Vistascope from Molecular Vista, Inc. We customize the commercial Si AFM probes with a cantilever and tip from Nanosensor (PPP-NCHR), which exhibits a 330 kHz nominal mechanical resonance frequency. We deposit an approximately 45 nm gold layer by sputtering on the Si tip, which gives the best SNR according to our optimization test. The schematic of the PiFM

DOI: 10.1021/acsnano.8b05778
ACS Nano 2018, 12, 12159−12168

is shown in Figure 1, where in the present configuration, the test sample is represented by a Si truncated cone and the illumination beam is an APB. Our PiFM instrument contains two scanning modes, that is, sample and objective scanning modes. In both modes, the transverse position of the tip is always fixed. In the sample scanning mode, a raster scan is performed for the sample stage, while the incident beam is stationary; whereas in the objective scanning mode, the raster scan is performed for the bottom objective lens that effectively scans the incident beam, while the sample stays stationary. The PiFM performs in the dynamic attractive mode to characterize the photoinduced force in the longitudinal direction (z direction according to Figure 1) for all force measurements discussed in this work. The force amplitude is measured in unit of volts as the readout from the photodetector. We set the second resonance frequency (about 2 MHz) of the cantilever as the drive frequency for mechanical oscillation and the first resonance frequency (330 kHz) as the detection frequency for photoinduced force, to utilize the high-quality factor of the first resonance for improving SNR. Also, we set the default drive amplitude and the engaging set point of the cantilever to the sample surface as 2 nm and 85% (resulting in a 1.7 nm oscillation amplitude when tip and sample are engaged), respectively. Starting from the default value, we slightly adjust these parameters in specific measurements to maximize the SNR.

Silicon Truncated Cone under APB Illumination. Since most common natural materials are not magnetically responsive at optical frequencies, we seek solutions of making the magnetic structure by using nanostructures with artificial optical magnetism.[31−45] As an appropriate candidate, the Mie resonances of dielectric nanostructures provided by the displacement currents grant artificial optical magnetism.[35−44,46−49] Indeed, based on the Mie theory for light scattering by subwavelength objects, the refractive index, the size, and the shape of the scatterer define the resonance frequency of each mode.[50−52] Here, we choose a Si truncated cone with a Mie-type magnetic resonance as the magnetic structure to exploit its structural simplicity, low loss, and versatility in the design. Note that there is no particular physical reason to make a tilted wall of the Si structure to make it a "truncated cone". A "disk" structure can also support the magnetic Mie resonance. However, because the realistic fabrication always induces a tilted wall of the disk, the "truncated cone" is a more proper name to describe this structure.

To selectively induce the magnetic mode of the Si truncated cone, we propose to illuminate it by an axis-aligned APB system.[31,53−55] An APB possesses a purely transverse electric field that circulates around the beam axis.[56,57] Such a circulating electric field induces a strong oscillating longitudinal magnetic field with a vanishing electric field at the beam axis.[2,45,56−58] While placing the Si truncated cone, which is azimuthally symmetric on-axis with the APB, we expect that at the designed resonance frequency of the magnetic mode, the magnetic dipole of the Si truncated cone is exclusively excited due to the symmetry of the illumination beam. Because of the azimuthal symmetry of both the Si truncated cone and its illumination, around the shared axis of symmetry (the z-axis), only the magnetic field should be nonvanishing and enhanced.[54,55] As a result, the combination of Si truncated cone and the APB illumination system is a judicious solution to characterize the optical magnetism in such structure. Similar ideas of achieving selective magnetic excitation by employing a magnetic resonator with its axis-aligned to an APB illumination have also been recently explored.[2,45,59] In addition, here we also exploit the standing wave created by two obliquely incident counter-propagating plane waves with matching polarization that can also induce a local magnetic dominant region for exclusive magnetic excitation.[16,60−62] This standing wave illumination, though very convenient for numerical investigations, is not practical in our PiFM experimental system setups which employ an inverted microscope optical system with limited flexibility for modifications, besides the difficulty one would have in the control of the phase of each plane wave. We eventually choose the Si truncated cone with APB illumination combination based on the consideration of both fabrication and optical experimental characterization convenience.

Following our previous studies,[54,55] to express the efficiency of the Si truncated cone as an efficient magnetic resonant structure, we consider two figures of merit (FOMs) F_H and F_Y, respectively, as the local magnetic field enhancement and the normalized (to the wave impedance of a plane wave) local field admittance, defined by[31,55]

$$F_H = \frac{|\mathbf{H}^t(\mathbf{r})|}{|\mathbf{H}^i(\mathbf{r})|}, \qquad F_Y = \eta\frac{|\mathbf{H}^t(\mathbf{r})|}{|\mathbf{E}^t(\mathbf{r})|} \tag{1}$$

Here, $|\mathbf{H}^t(\mathbf{r})|$, $|\mathbf{E}^t(\mathbf{r})|$, and $|\mathbf{H}^i(\mathbf{r})|$ are the absolute values of the total magnetic, electric, and the incident magnetic field at position $\mathbf{r}$, respectively, while η represents the plane wave impedance in vacuum. The magnetic field enhancement F_H implies the capability of the magnetic resonant structure to boost the local magnetic field with respect to the incident one. The normalized local field admittance F_Y indicates the ratio between the total magnetic and electric field. Any value larger than unity indicates structured light with dominant magnetic field compared to the case of a plane wave.

The Si truncated cone discussed in this paper is deposited on a glass substrate to resonate at 670 nm, that is, the wavelength of our laser source. The verification is done by full-wave simulations based on the time-domain finite integration technique (FIT) implemented in the commercial software CST Microwave Studio by Computer Simulation Technology AG. Since the magnetic resonance frequency of the Si truncated cone is independent of the excitation type, for simplicity and time efficiency purposes, we apply a simplified procedure to obtain appropriate dimensions of the Si truncated cone on the glass substrate to achieve a magnetic resonance at 670 nm. Indeed, we illuminate the Si truncated cone with two counter-propagating plane waves (rather than an APB) possessing antisymmetric electric field with respect to the truncated cone longitudinal axis, shown in Figure 2a, to provide a standing electromagnetic wave with vanishing electric field at the truncated cone center where a maximum of longitudinal magnetic field occurs.[31] Note that due to the presence of the substrate, it is not possible to use the standard Mie theory for the calculation of Mie coefficients. Moreover, the presence of the substrate forces us to apply oblique illumination in the used full-wave software rather than tangential illumination from each side of the truncated cone. We used the two counter-propagating plane waves as excitation to retrieve the resonant wavelength of the Si truncated cone structure and design its appropriate dimensions to exhibit a resonance in proximity of our laser wavelength, that is, 670 nm.

DOI: 10.1021/acsnano.8b05778
ACS Nano 2018, 12, 12159−12168

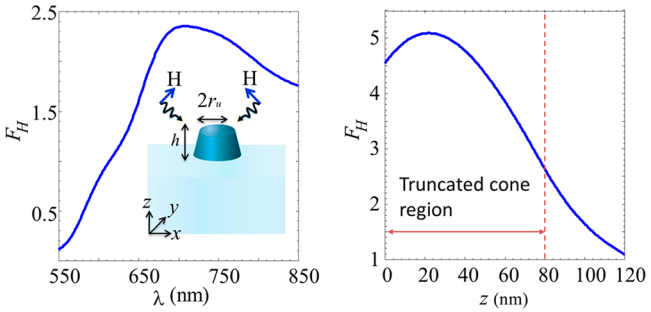

Figure 2. Magnetic field enhancement at the truncated cone axis: (a) observation 5 nm above the truncated cone top surface *versus* wavelength, and (b) *versus* changing observation point along the truncated cone axis at the fixed wavelength of 670 nm. The structure is excited with two counter propagating plane waves with ±45° incident angle to the *z*-axis to create maximum magnetic field and zero electric field along the truncated cone axis. The upper radius and lower radius are denoted as r_u and r_l, respectively. The designed Si truncated cone has height h = 80 nm and is placed on top of a glass substrate, and the truncated cone−substrate interface is at z = 0.

The simulated field distribution investigated in this paper was measured using the realistic illuminations in our experimental setup, that is, a APB coming from the bottom of the system.[55] The relative permittivity of Si is acquired from spectroscopic ellipsometry characterization service from the company J. A. Woollam based on a sputter-coated 80 nm-thick Si film on glass coverslip, leading to a Si relative permittivity of 9.5+i1.1 at 670 nm. The fabricated Si truncated cone has a truncated cone shape rather than a perfect cylinder. Therefore, to include the fabrication imperfections in our simulation design, we consider the Si truncated cone shape with the upper radius of r_u = 100 nm, the lower radius of r_l = 135 nm, with height of h = 80 nm, according to the measured topography from AFM shown in Figure 3b,c. Based on our numerical calculations, such a design provides a magnetic resonance approximately at 670 nm. Figure 2a shows the magnetic field enhancement F_H *versus* incident light wavelength generated by the Si truncated cone on glass substrate, when the structure is excited with two TE-to-*z* plane waves with antisymmetrical electric fields that vanish at the truncated cone axis. The oblique angles of the two incident beams are ±45° to the *z*-axis, respectively. The point where the field is evaluated, which represents the approximate position of the tip, is set to be 5 nm above the top surface of the truncated cone, on the truncated cone symmetry axis. Figure 2b shows the magnetic field enhancement along the Si truncated cone axis (*i.e.*, along the *z*-axis) at the magnetic resonance wavelength 670 nm. The starting point (*i.e.*, z = 0) is the interface between the Si truncated cone and the glass substrate. Our results show that the magnetic field is strongest inside the Si truncated cone, near the glass substrate (at $z \approx 20$ nm). We attribute this phenomenon to two reasons: First, the bottom of the Si truncated cone (truncated cone) is wider than its top. Second, the presence of the glass substrate, which has higher refractive index compared to air, modifies the field distribution inside the Si truncated cone and leads to a higher field concentration at locations closer to the Si−glass interface rather than Si−vacuum interface.[63−66] According to our simulation results, by moving the observation point (or equivalently the tip location in the PiFM paradigm) away from the truncated cone−vacuum interface along its axis, the local magnetic field diminishes rapidly, and there would be almost no magnetic field enhancement (*i.e.*, F_H = 1) just 40 nm away from the truncated cone surface.

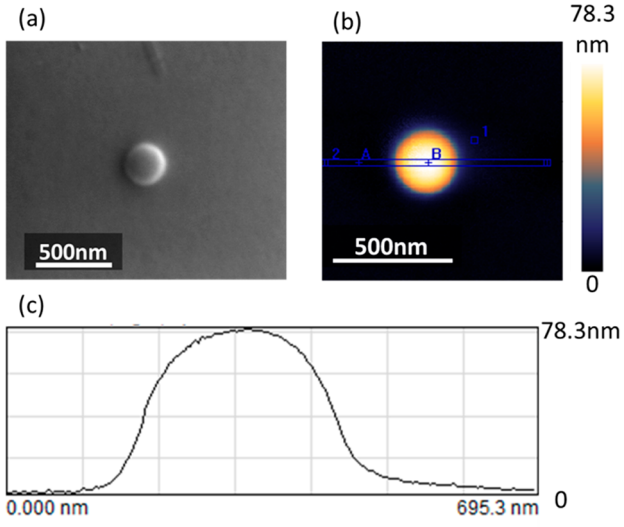

Figure 3. (a) The SEM image of the fabricated Si truncated cone on a glass slip. (b) The AFM topography of the fabricated Si truncated cone on the glass slip. (c) The cross-section height profile of the Si truncated cone along the blue stripe line in (b).

The Si truncated cone fabrication is performed by depositing a 80 nm-thick undoped amorphous Si film on a glass slip by sputter deposition and then using a focused ion beam (FIB) to remove the undesired background, leaving the desired standing Si truncated cone. Figure 3 shows the scanning electron microscopy (SEM) image and AFM topography of the fabricated Si truncated cone. It is noteworthy that due to the top-down milling fabrication technique, even if we wanted to fabricate a straight "disk" structure, its side wall is always slightly tilted, which makes a larger bottom width compared to the top width. As mentioned above, we have named it as Si truncated cone and have applied the measured dimensions of the fabricated Si truncated cone in the simulation discussed previously to improve the accuracy of numerical predictions.

EXPERIMENTS AND INTERPRETATIONS

To study the Si truncated cone under APB illumination, we begin with the characterization of a tightly focused APB. To this end, we generate the required APB with a power of about 150 μW by having a linearly polarized beam passing through a commercial azimuthal polarizer from the company ARCoptix[67] with a very symmetric intensity profile[17] and then focus it through a bare glass slip using an oil immersion high numerical aperture (NA) objective lens. The laser source used here is a continuous wave (CW) single mode fiber pigtailed laser diode at 670 nm. We perform the PiFM measurements with an objective scan (PiFM tip and glass slip stay fixed) and compare it with full-wave simulation results. The measured force map of the focused APB exhibits a clear donut shape with subwavelength features as shown in Figure 4a. We define the SNR of the measured force map as the maximum of the measurement related to force amplitude, 1.402 mV in our experiment, divided by the average background amplitude measured at the detector, about 0.02 mV, which results in a value of the nanoscale near-field SNR measurement of 70:1. And we recall that the power of the incident tightly focused

DOI: 10.1021/acsnano.8b05778
ACS Nano 2018, 12, 12159−12168

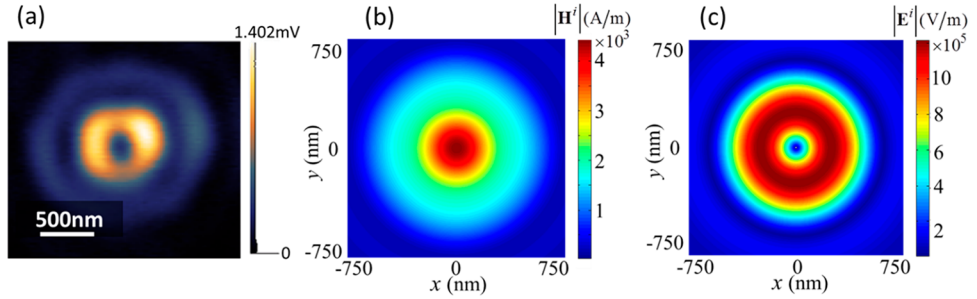

Figure 4. (a) Measured force map of the sharply focused APB. (b, c) Full-wave calculated magnetic and electric field profiles of the incident APB evaluated at z = 85 nm. The APB focal plane is at z = 0.

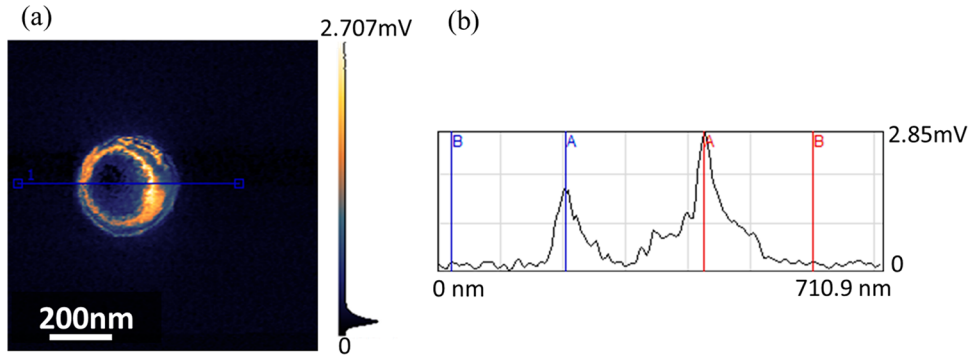

Figure 5. (a) Measured force map of the Si truncated cone under APB illumination with the blue line representing for the cross-line. (b) The cross-line of the measured force. In this measurement, tip and incident APB are aligned and fixed, while the stage with the Si truncated cone is moving.

structured light is about 150 μW. Note that the center of the APB does not exhibit the exact minimum (background) force. This is because the effective tip-apex has a finite dimension so that when the tip and the incident APB are aligned, the tip-apex will cover more than the exact axis of the APB. As a result, the total force exerted on the tip will be larger than zero.

The relationship between the measured photoinduced force and the local electric field of APB is discussed in detail in our previous work.[17] Thanks to its azimuthal symmetry without longitudinal electric field, the APB is a simple but useful form of structured light for our purpose. For a perfectly azimuthally symmetric tip-apex in PiFM, the photoinduced force exerted on the tip is proportional to the gradient of the local electric field in the presence of the tip, which is also proportional to the field intensity of the incident APB, as shown in ref 17 for a realistic asymmetric tip-apex, the photoinduced force will exhibit tip-induced anisotropy according to the anisotropic transverse polarizability of the effective tip dipole.[17] This is the reason why the force map in Figure 4a exhibits an asymmetric donut shape. Such an anisotropy effect can be analyzed and retrieved by establishing a numerical model which takes the azimuthal averaging from the experimental force map.[17]

In the simulations, the required incident APB is generated by implementing an in-house developed code[57] and then imported into the commercial CST Microwave Studio software tool as a field source which propagates along the + z direction, that is, from the substrate toward the sample.[56,57] The beam characteristics are assumed to be as follows: Wavelength is 670 nm, beam parameters w_0 which is defined in ref 57 as the minimum waist of the donut shape APB is 469 nm ($w_0 = 0.7\lambda$), and the power intensity is 1 mW. The focal plane of the incident APB is the transverse plane at z = 0. Figure 4b,c, respectively, exhibits the profile of the absolute amplitude of the incident magnetic and electric fields at the transverse observation plane at z = 85 nm, which is the equivalent plane to show the field distribution 5 nm above the Si truncated cone located on a glass substrate (the interface of the Si truncated cone and the glass substrate is at z = 0). The simulations show a perfect donut shape for the incident electric field and a center focused magnetic field as the expected features of an APB, confirming the experimental results.

Next, we characterize the Si truncated cone under the APB illumination by PiFM using stage scanning. In this measurement, we first align the tip to the APB axis by moving the objective lens, then align the Si truncated cone axis to the center of the beam by moving the sample stage, and last scan the sample around the tip by the sample scanning mechanism as explained before. The measured force map of the Si truncated cone under the APB illumination is shown in Figure 5.

It is noteworthy that the sample scanning mechanism and data interpretation are nontrivial, since the sample stage is moving while the objective lens and tip are fixed at the same transverse position, aligned to each other. This means the Si truncated cone and the beam do not stay aligned during the sample scanning. To provide a better understanding of the measured data, we have performed a series of simulations to reflect the realistic experimental scenarios. Starting from the scenario when the axes of the Si truncated cone and incident APB are perfectly aligned, we show the simulated electric and magnetic field distributions of the Si truncated cone under APB illumination in Figure 6. The full-wave simulation results of the total electric field in Figure 6a,b and the total magnetic field in Figures 6c,d are shown in two cutting planes, that is,

DOI: 10.1021/acsnano.8b05778
ACS Nano 2018, 12, 12159−12168

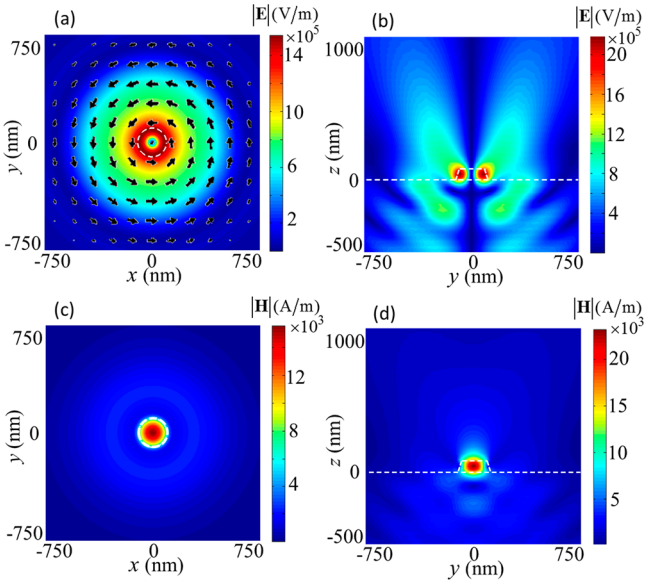

Figure 6. Simulation results with Si truncated cone and surface marked by white dashed lines: (a) Local electric field distribution at the transverse (x–y) plane 5 nm above the top plane of the Si truncated cone, with the direction of the electric field at a given time shown in arrows. (b) Magnitude of the electric field distribution at the longitudinal (y–z) plane containing the truncated cone axis; the section of the glass substrate and the Si truncated cone is visible. (c, d) Magnitude of the magnetic field distribution at the same transverse and longitudinal planes as in (a) and (b), respectively.

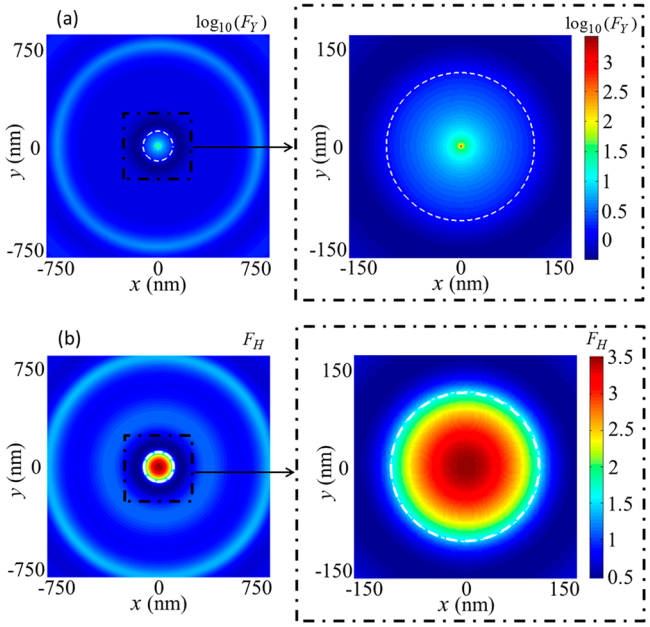

Figure 7. Simulation results: (a, b) Local magnetic field enhancement F_H and the normalized local field admittance F_Y at the (x–y) transverse plane, 5 nm above the top plane of the Si truncated cone. The right side figures are the zoomed-in magnification of the center part of the left side figures. The top radius of the Si truncated cone is marked with a white dashed circle.

the transverse plane 5 nm above the truncated cone top surface (z = 85 nm) and the longitudinal cross section plane passing the truncated cone center (y–z plane). As mentioned previously, the interface between the glass substrate and the Si truncated cone is placed at the focal plane of the incident APB, that is, the transverse plane at z = 0. It is clear from these figures that the magnetic field has a hot-spot at the truncated cone center, while the electric field is circulating the center axis with a donut shape profile peaking around the edge of the truncated cone. This is exactly as it is theoretically expected for the magnetic resonance behavior of a dielectric scatterer with a circular displacement current and the oscillating longitudinal magnetic field at the center.[36] To further confirm the magnetic dominant behavior of the designed Si truncated cone at 670 nm, we show the normalized local field admittance F_Y and the magnetic field enhancement F_H in Figure 7a,b, respectively. The incident values in Figures 7 to evaluate these two figures of merit are calculated without Si truncated cone and with glass substrate. These results indicate both a strong enhancement of the normalized local magnetic to electric field ratio (F_Y = 1000 at the Si axis, 5 nm above the Si truncated cone top surface) and a strong local enhancement of the magnetic field (F_H = 3.5 at the beam axis, 5 nm above the Si truncated cone top surface). As discussed earlier, the values of these two FOMs together with the electric/magnetic field distributions shown in Figure 6 demonstrate that the Si truncated cone under such an illumination serves as an efficient magnetic structure.

Next, in Figure 8 we study the scenario of misalignment between the axis of the Si truncated cone and that of the incident APB. For this purpose, we introduce a displacement between the Si truncated cone and the incident APB axes to address the misalignment in the realistic experimental system, resulting from the stage scanning. We plot the electric field distribution in a transverse plane at 5 nm above the top surface of the Si truncated cone in two cases, that is, (1) when the truncated cone and the beam are exactly aligned (Figure 8a); and (2) when the Si truncated cone is displaced by 100 nm (the top radius of the truncated cone) with respect to the APB axis (Figure 8b). The local electric field distributions in both the aligned and misaligned cases clearly demonstrate magnetic responses because of the electric field vortex. Next, to quantify the effect of the Si displacement on the local electric field measurement, in Figure 8c,d, we plot the local magnetic field enhancement F_H and the normalized local field admittance F_Y at the (x–y) transverse plane, 5 nm above the top plane of the Si truncated cone with the misaligned axes. In Figure 8e, we plot the simulated electric field square magnitude $|\mathbf{E}|^2$ at the observation point, x = 0, z = 85 nm, which is 5 nm above the top surface of the Si truncated cone, *versus* the x-displacement, that is, the lateral displacement during the stage scan. The local electric field evaluated at x = 0 shows a peak when the displacement equals the truncated cone upper radius. This demonstrates that the magnetic response of the Si truncated cone is preserved even with a small misalignment between the truncated cone and the incident APB. We recall that the Si truncated cone has an upper radius r_u = 100 nm, which is significantly smaller than the beam parameter $w_0 = 0.7\lambda$ = 496 nm at the focal plane z = 0, also the bottom plane of the Si truncated cone. Considering such a displacement analysis as a representative of our sample scan (*i.e.*, stage scan), the result in Figure 8e shows agreement between the simulated square magnitude of the electric field and the experimental measured force map using the PiFM shown in Figure 8e for convenience of comparison.

DOI: 10.1021/acsnano.8b05778
ACS Nano 2018, 12, 12159–12168

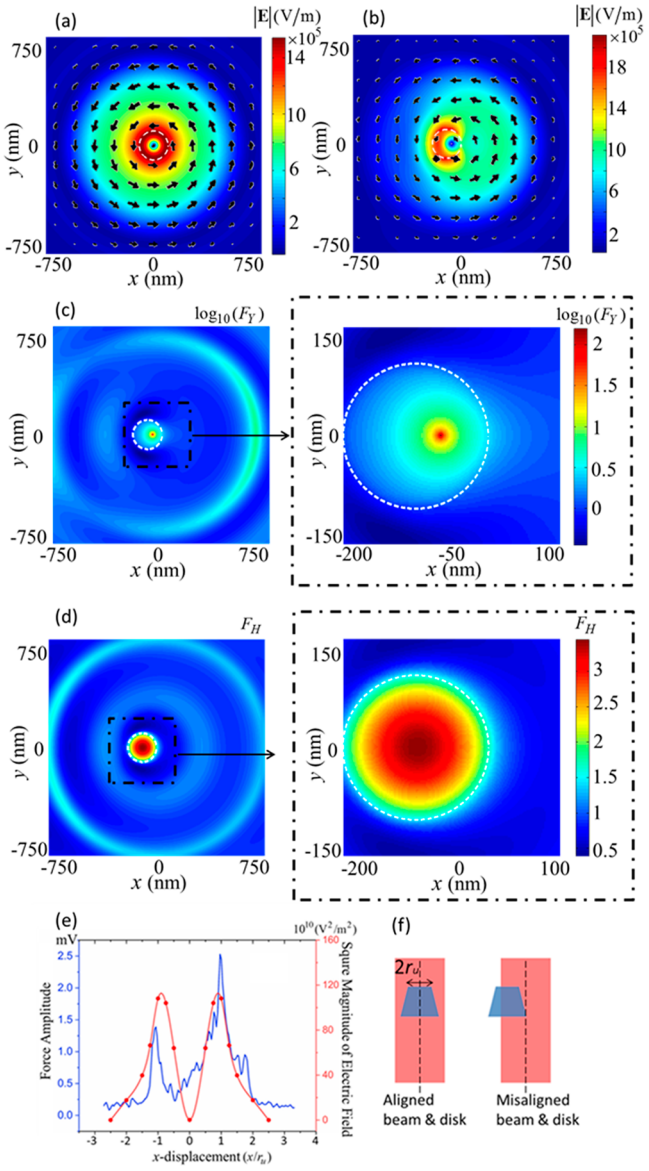

Figure 8. Simulation results: (a, b) Electric field at the transverse plane, 5 nm above the top surface of the Si truncated cone, with aligned and misaligned axes between the incident beam and the Si truncated cone, respectively, where the arrows represent the electric field vector at a given time. The center of the APB is always at $x = 0$, and the truncated cone is translated (as in a stage scan). (c, d) Local magnetic field enhancement F_H and the normalized local field admittance F_Y at the (x–y) transverse plane, 5 nm above the top plane of the Si truncated cone with the misaligned axes. The right side figures are the zoomed-in magnification of the center part of the left side figures. The top radius of the Si truncated cone is marked with a white dashed circle. (e) Simulated square magnitude of electric field $|E|^2$ (red curve) at $x = 0$ (*i.e.*, on the beam axis), 5 nm above the top surface of the Si truncated cone, *versus* x-displacement of the Si truncated cone from the APB axis. We also report the measured force amplitude (blue curve) *versus* x-displacement, from Figure 5b, for comparison. (f) Schematic of the aligned and misaligned Si truncated cone with respect to the APB axis.

We further analyze the results of our PiFM experiment in Figure 5a. Taking a closer look at the force map of the Si truncated cone under the APB illumination, we can see there are two annular bright rings around the truncated cone edge. We attribute them to field concentrations at the top edge and the bottom edge of the truncated cone, respectively, due to the tilted side wall. The force map shows several small detailed features around the edge of the truncated cone, demonstrating an ultrafine resolution down to sub-10 nm. Furthermore, the SNR ratio, as defined previously as the maximum of the measurement related to force amplitude, here 2.707 mV, divided by the average background amplitude measured at the detector, about 0.02 mV, reaches 130:1. Recalling the incident beam power which is about 150 μW, the measured force map of the illuminated nanostructure by PiFM exhibits superior resolution and SNR compared to any other methods that we know, for example, the NSOM.[68,69] Moreover, we observe certain asymmetry in the measured force map. Based on our best understanding of the PiFM system, we present three major reasons for such an asymmetry: (1) the realistic tip-apex with anisotropic transverse polarizability, which will create a different field-to-force response for different transverse polarization components;[17] (2) the imperfect surface in the fabricated Si truncated cone, which may induce a non-uniform local field-to-force response; (3) the alignment error between the tip and the APB axis while performing the sample scanning. We expect the asymmetry can be efficiently eliminated in the near future when we adopt an improved deposition technique to make a more symmetric tip-apex, a revised fabrication technique to make a more uniform truncated cone, and a more accurate positioning mechanism in the PiFM system.

Lastly, we interpret the PiFM measurement in Figure 5 and relate it to the magnetic excitation of the Si truncated cone structure. As a general principle, to completely resolve an arbitrarily unknown light–matter interaction, which means retrieving the amplitude, polarization, and phase of the local field, one needs to measure at least three mutually independent parameters.[70] In this perspective, since our PiFM can only directly measure the longitudinal photoinduced electric force exerted on the probe-tip that counts as one independent measurement, the current method cannot resolve an unknown light–matter interaction system as a black box. However, if the interested light–matter interaction is well-defined, a physical model can be created to represent such an interaction. Then, if a certain measurable physical quantity predicted by the model, such as light intensity distribution, scattering spectrum, *etc*, shows a reasonable agreement with the experimental measurement, we can use the matching model as the physical representation of the realistic light–matter interaction and consider all calculated physical quantities based on the model as the experimentally retrieved results. This principle has been widely applied in the application of ellipsometry and optical frequency metamaterials effective index retrieval.[71,72]

Here, we apply the matching modeling principle for our Si truncated cone structure under APB illumination. Let us have a brief review of the steps to characterize the optical magnetism of the structure. First, we acquired the dimension of the fabricated truncated cone structure from AFM topography measurement, the relative permittivity of Si from ellipsometry measurement, and the beam profile of the incident sharply focused APB from PiFM measurement. Then, we employed these parameters to model such an optical system using full-wave simulations (here, the finite element method implemented in CST MWS) to determine its electromagnetic properties as shown in Figures 6–8. Next, we perform the displacement study to simulate the electric field in the position of an imaginary probe *versus* the displacement distance

DOI: 10.1021/acsnano.8b05778
ACS Nano 2018, 12, 12159–12168

between the structure and the beam axis to mimic the sample scan mechanism of the PiFM (*i.e.*, mimic the stage scan). As shown in Figure 8e, the simulated square magnitude of electric field has an excellent fit to the trend of the measured photoinduced force, which is as expected in theory.[17] Therefore, we consider this model as an eligible interpretation of the experiment measurement. Using this model, we plotted the normalized local field admittance and magnetic field enhancement in Figure 7. It shows a larger than unity magnetic field enhancement and an extremely large magnetic-to-electric field ratio near the axis of the structure, which are the signatures of the dominant magnetic response.

The above results provide a compact picture of the magnetic excitation in our structure. In addition, we also perform an in-depth multipole analysis to quantitatively show the contributions of the multipoles to the total scattered power under different conditions for comparison. The analysis includes the cases of a Si truncated cone aligned or misaligned with an incident APB and also the cases of a Si truncated cone with either a plane wave or a standing wave excitation (please refer to the Supporting Information for this content). In short, we reached the conclusion that our proposed Si truncated cone structure with an aligned APB illumination achieves an excellent exclusively magnetic excitation with both high efficiency and convenience over a wide frequency range around the magnetic resonance of the structure.

CONCLUSIONS

We have presented a characterization of the electric near-field distribution generated by a Si truncated cone under tightly focused APB illumination by using PiFM with a superior resolution and SNR. Our measurements show a donut shape electric near-field profile around the truncated cone edge while performing a stage scan, which agrees with the numerical simulations and indicates the exclusive magnetic response of the proposed system. Such a Si truncated cone resonator can serve as a plausible magnetic nanoprobe at optical frequencies. Within this vision, the Si truncated cone magnetic nanoprobe could be placed at the end of a force microscope nanotip, and magnetic near-field at optical frequency could be detected by photoinduced magnetic force as theoretically predicted in previous work.[54,55] Moreover, such a methodology can be further extended to investigate other types of structured light beams, structured materials such as metamaterials and metasurfaces, and natural materials with magnetic dipolar transitions such as lanthanide-doped nanostructures.[1,2]

METHODS

We use the sputter-coater from South-bay Technology Inc. with a Si target from Kurt J. Lesker Company to deposit an undoped, amorphous Si film on a glass coverslip. Then we use focus ion beam (FIB) lithography to fabricate the standing Si truncated cone structure by using the Quanta scanning electron microscope (SEM) system from FEI Thermo Fisher Scientific. The relative permittivity of the deposited Si and the glass substrate is characterized by ellipsometry through a service contract with J. A. Woollam Co. We use the continuous wave (CW) single mode fiber pigtailed laser diode at 670 nm from Thorlabs Inc. as light source and the polarization converter from the company ARCoptix to produce the APB. Finally, we characterize the surface topography and photo-induced force profile of the Si truncated cone with the substrate by using the Vistascope PiFM from Molecular Vista Inc. Numerical simulations are carried out by using the full-wave simulation tool provided by Computer Simulation Technology (CST) of America, Inc. based on the finite element method.

ASSOCIATED CONTENT

Supporting Information

The Supporting Information is available free of charge on the ACS Publications website at DOI: 10.1021/acsnano.8b05778.

Discussions regarding the quantitative contributions of the multipoles associated with the illuminated Si truncated cone to the total scattered power under different illumination conditions (PDF)

AUTHOR INFORMATION

Corresponding Authors

*E-mail: epotma@uci.edu.
*E-mail: f.capolino@uci.edu.
*E-mail: hkwick@uci.edu.

ORCID

Jinwei Zeng: 0000-0001-5795-2406
Mohsen Rajaei: 0000-0001-8918-5539
Mohammad Kamandi: 0000-0002-9135-8686
Eric O. Potma: 0000-0003-3916-6131

Author Contributions

E.P., F.C., and H.K.W. conceived the main idea of this work. J.Z. and M.R. performed the fabrication and experimental characterization. M.D., M.A., M.K., and M.V. performed the theoretical calculation and numerical simulations. All authors wrote and approved the manuscript.

Funding

W. M. Keck Foundation (USA). NSF Center for Chemical Innovation - Chemistry at the Space-Time Limit (CHE-1414466).

Notes

The authors declare no competing financial interest.

ACKNOWLEDGMENTS

The authors would like to thank Computer Simulation Technology (CST) of America, Inc. for providing CST Microwave Studio, which was instrumental in this work.

REFERENCES

(1) Dodson, C. M.; Zia, R. Magnetic Dipole and Electric Quadrupole Transitions in the Trivalent Lanthanide Series: Calculated Emission Rates and Oscillator Strengths. *Phys. Rev. B: Condens. Matter Mater. Phys.* **2012**, *86*, 125102.

(2) Kasperczyk, M.; Person, S.; Ananias, D.; Carlos, L. D.; Novotny, L. Excitation of Magnetic Dipole Transitions at Optical Frequencies. *Phys. Rev. Lett.* **2015**, *114*, 163903.

(3) Hauptmann, N.; Gerritsen, J. W.; Wegner, D.; Khajetoorians, A. A. Sensing Noncollinear Magnetism at the Atomic Scale Combining Magnetic Exchange and Spin-Polarized Imaging. *Nano Lett.* **2017**, *17*, 5660−5665.

(4) Antoniak, C.; Gruner, M. E.; Spasova, M.; Trunova, A. V.; Römer, F. M.; Warland, A.; Krumme, B.; Fauth, K.; Sun, S.; Entel, P.; Farle, M.; Wende, H. A Guideline for Atomistic Design and Understanding of Ultrahard Nanomagnets. *Nat. Commun.* **2011**, *2*, 528.

DOI: 10.1021/acsnano.8b05778
ACS Nano 2018, 12, 12159−12168

(5) Stanciu, C. D.; Hansteen, F.; Kimel, A. V.; Kirilyuk, A.; Tsukamoto, A.; Itoh, A.; Rasing, T. All-Optical Magnetic Recording with Circularly Polarized Light. *Phys. Rev. Lett.* **2007**, *99*, 047601.
(6) Neuman, K. C.; Nagy, A. Single-Molecule Force Spectroscopy: Optical Tweezers, Magnetic Tweezers and Atomic Force Microscopy. *Nat. Methods* **2008**, *5*, 491−505.
(7) Souza, G. R.; Molina, J. R.; Raphael, R. M.; Ozawa, M. G.; Stark, D. J.; Levin, C. S.; Bronk, L. F.; Ananta, J. S.; Mandelin, J.; Georgescu, M.-M.; et al. Three-Dimensional Tissue Culture Based on Magnetic Cell Levitation. *Nat. Nanotechnol.* **2010**, *5*, 291−296.
(8) Cook, J. J. H.; Tsakmakidis, K. L.; Hess, O. Ultralow-Loss Optical Diamagnetism in Silver Nanoforests. *J. Opt. A: Pure Appl. Opt.* **2009**, *11*, 114026.
(9) Martin, Y.; Wickramasinghe, H. K. Magnetic Imaging by '"Force Microscopy"'with 1000 \AA Resolution. *Appl. Phys. Lett.* **1987**, *50*, 1455−1457.
(10) Gao, D.; Ding, W.; Nieto-Vesperinas, M.; Ding, X.; Rahman, M.; Zhang, T.; Lim, C.; Qiu, C.-W. Optical Manipulation from the Microscale to the Nanoscale: Fundamentals, Advances and Prospects. *Light: Sci. Appl.* **2017**, *6*, e17039.
(11) Monticone, F.; Alù, A. The Quest for Optical Magnetism: From Split-Ring Resonators to Plasmonic Nanoparticles and Nanoclusters. *J. Mater. Chem. C* **2014**, *2*, 9059−9072.
(12) Landau, L. D.; Lifshits, E. M. *Course of Theoretical Physics: Electrodynamcis of Continuous Media*; Pergamon Press: Oxford, 1960.
(13) Burresi, M.; Van Oosten, D.; Kampfrath, T.; Schoenmaker, H.; Heideman, R.; Leinse, A.; Kuipers, L. Probing the Magnetic Field of Light at Optical Frequencies. *Science* **2009**, *326*, 550−553.
(14) Giessen, H.; Vogelgesang, R. Glimpsing the Weak Magnetic Field of Light. *Science* **2009**, *326*, 529−530.
(15) Taminiau, T. H.; Karaveli, S.; Van Hulst, N. F.; Zia, R. Quantifying the Magnetic Nature of Light Emission. *Nat. Commun.* **2012**, *3*, 979.
(16) Kihm, H. W.; Koo, S. M.; Kim, Q. H.; Bao, K.; Kihm, J. E.; Bak, W. S.; Eah, S. H.; Lienau, C.; Kim, H.; Nordlander, P.; Halas, N. J.; Park, N. K.; Kim, D. -S. Bethe-Hole Polarization Analyser for the Magnetic Vector of Light. *Nat. Commun.* **2011**, *2*, 451.
(17) Zeng, J.; Huang, F.; Guclu, C.; Veysi, M.; Albooyeh, M.; Wickramasinghe, H. K.; Capolino, F. Sharply Focused Azimuthally Polarized Beams with Magnetic Dominance: Near-Field Characterization at Nanoscale by Photoinduced Force Microscopy. *ACS Photonics* **2018**, *5*, 390−397.
(18) Rajapaksa, I.; Uenal, K.; Wickramasinghe, H. K. Image Force Microscopy of Molecular Resonance: A Microscope Principle. *Appl. Phys. Lett.* **2010**, *97*, 073121.
(19) Martin, Y.; Williams, C. C.; Wickramasinghe, H. K. Atomic Force Microscope−Force Mapping and Profiling on a Sub 100-\AA Scale. *J. Appl. Phys.* **1987**, *61*, 4723−4729.
(20) Nonnenmacher, M.; o'Boyle, M. P.; Wickramasinghe, H. K. Kelvin Probe Force Microscopy. *Appl. Phys. Lett.* **1991**, *58*, 2921−2923.
(21) Tumkur, T. U.; Yang, X.; Cerjan, B.; Halas, N. J.; Nordlander, P.; Thomann, I. Photoinduced Force Mapping of Plasmonic Nanostructures. *Nano Lett.* **2016**, *16*, 7942−7949.
(22) Tumkur, T.; Yang, X.; Zhang, C.; Yang, J.; Zhang, Y.; Naik, G. V.; Nordlander, P.; Halas, N. J. Wavelength-Dependent Optical Force Imaging of Bimetallic Al−Au Heterodimers. *Nano Lett.* **2018**, *18*, 2040−2046.
(23) Huang, F.; Tamma, V. A.; Mardy, Z.; Burdett, J.; Wickramasinghe, H. K. Imaging Nanoscale Electromagnetic Near-Field Distributions Using Optical Forces. *Sci. Rep.* **2015**, *5*, 10610.
(24) Nowak, D.; Morrison, W.; Wickramasinghe, H. K.; Jahng, J.; Potma, E.; Wan, L.; Ruiz, R.; Albrecht, T. R.; Schmidt, K.; Frommer, J.; et al. Nanoscale Chemical Imaging by Photoinduced Force Microscopy. *Sci. Adv.* **2016**, *2*, e1501571.
(25) Jahng, J.; Brocious, J.; Fishman, D. A.; Huang, F.; Li, X.; Tamma, V. A.; Wickramasinghe, H. K.; Potma, E. O. Gradient and Scattering Forces in Photoinduced Force Microscopy. *Phys. Rev. B: Condens. Matter Mater. Phys.* **2014**, *90*, 155417.
(26) Huang, F.; Tamma, V. A.; Rajaei, M.; Almajhadi, M.; Kumar Wickramasinghe, H. Measurement of Laterally Induced Optical Forces at the Nanoscale. *Appl. Phys. Lett.* **2017**, *110*, 063103.
(27) Garrett, J. L.; Krayer, L. J.; Palm, K. J.; Munday, J. N. Effect of Lateral Tip Motion on Multifrequency Atomic Force Microscopy. *Appl. Phys. Lett.* **2017**, *111*, 043105.
(28) Kim, B.; Jahng, J.; Khan, R. M.; Park, S.; Potma, E. O. Eigenmodes of a Quartz Tuning Fork and Their Application to Photoinduced Force Microscopy. *Phys. Rev. B: Condens. Matter Mater. Phys.* **2017**, *95*, 075440.
(29) Kamandi, M.; Albooyeh, M.; Guclu, C.; Veysi, M.; Zeng, J.; Wickramasinghe, K.; Capolino, F. Enantiospecific Detection of Chiral Nanosamples Using Photoinduced Force. *Phys. Rev. Appl.* **2017**, *8*, 064010.
(30) Rajaei, M.; Almajhadi, M. A.; Zeng, J.; Wickramasinghe, H. K. Near-Field Nanoprobing Using Si Tip-Au Nanoparticle Photoinduced Force Microscopy with 120:1 Signal-to-Noise Ratio, Sub-6-Nm Resolution. *Opt. Express* **2018**, *26*, 26365−26376.
(31) Darvishzadeh-Varcheie, M.; Guclu, C.; Capolino, F. Magnetic Nanoantennas Made of Plasmonic Nanoclusters for Photoinduced Magnetic Field Enhancement. *Phys. Rev. Appl.* **2017**, *8*, 024033.
(32) Thrift, W. J.; Darvishzadeh-Varcheie, M.; Capolino, F.; Ragan, R. Templated Electrokinetic Directed Chemical Assembly for the Fabrication of Close-Packed Plasmonic Metamolecules. In *Plasmonics: Design, Materials, Fabrication, Characterization, and Applications XV*; International Society for Optics and Photonics: San Diego, CA, 2017; Vol *103461*. DOI: 10.1117/12.2274554.
(33) Shalaev, V. M.; Cai, W.; Chettiar, U. K.; Yuan, H.-K.; Sarychev, A. K.; Drachev, V. P.; Kildishev, A. V. Negative Index of Refraction in Optical Metamaterials. *Opt. Lett.* **2005**, *30*, 3356−3358.
(34) Dolling, G.; Enkrich, C.; Wegener, M.; Zhou, J. F.; Soukoulis, C. M.; Linden, S. Cut-Wire Pairs and Plate Pairs as Magnetic Atoms for Optical Metamaterials. *Opt. Lett.* **2005**, *30*, 3198−3200.
(35) Alu, A.; Engheta, N. The Quest for Magnetic Plasmons at Optical Frequencies. *Opt. Express* **2009**, *17*, 5723−5730.
(36) Kuznetsov, A. I.; Miroshnichenko, A. E.; Fu, Y. H.; Zhang, J.; Luk'yanchuk, B. Magnetic Light. *Sci. Rep.* **2012**, *2*, 492.
(37) Campione, S.; Guclu, C.; Ragan, R.; Capolino, F. Enhanced Magnetic and Electric Fields *via* Fano Resonances in Metasurfaces of Circular Clusters of Plasmonic Nanoparticles. *ACS Photonics* **2014**, *1*, 254−260.
(38) Campione, S.; Lannebère, S.; Aradian, A.; Albani, M.; Capolino, F. Complex Modes and Artificial Magnetism in Three-Dimensional Periodic Arrays of Titanium Dioxide Microspheres at Millimeter Waves. *J. Opt. Soc. Am. B* **2012**, *29*, 1697−1706.
(39) Savelev, R. S.; Makarov, S. V.; Krasnok, A. E.; Belov, P. A. From Optical Magnetic Resonance to Dielectric Nanophotonics (A Review). *Opt. Spectrosc.* **2015**, *119*, 551−568.
(40) Permyakov, D.; Sinev, I.; Markovich, D.; Ginzburg, P.; Samusev, A.; Belov, P.; Valuckas, V.; Kuznetsov, A. I.; Luk'yanchuk, B. S.; Miroshnichenko, A. E.; et al. Probing Magnetic and Electric Optical Responses of Silicon Nanoparticles. *Appl. Phys. Lett.* **2015**, *106*, 171110.
(41) Staude, I.; Miroshnichenko, A. E.; Decker, M.; Fofang, N. T.; Liu, S.; Gonzales, E.; Dominguez, J.; Luk, T. S.; Neshev, D. N.; Brener, I.; Kivshar, Y. Tailoring Directional Scattering through Magnetic and Electric Resonances in Subwavelength Silicon Nanodisks. *ACS Nano* **2013**, *7*, 7824−7832.
(42) Kuznetsov, A. I.; Miroshnichenko, A. E.; Brongersma, M. L.; Kivshar, Y. S.; Luk'yanchuk, B. Optically Resonant Dielectric Nanostructures. *Science* **2016**, *354*, aag2472.
(43) Alaee, R.; Albooyeh, M.; Rahimzadegan, A.; Mirmoosa, M. S.; Kivshar, Y. S.; Rockstuhl, C. All-Dielectric Reciprocal Bianisotropic Nanoparticles. *Phys. Rev. B: Condens. Matter Mater. Phys.* **2015**, *92*, 245130.
(44) Krasnok, A. E.; Miroshnichenko, A. E.; Belov, P. A.; Kivshar, Y. S. All-Dielectric Optical Nanoantennas. *Opt. Express* **2012**, *20*, 20599−20604.

DOI: 10.1021/acsnano.8b05778
ACS Nano 2018, 12, 12159−12168

(45) Manna, U.; Lee, J.-H.; Deng, T.-S.; Parker, J.; Shepherd, N.; Weizmann, Y.; Scherer, N. F. Selective Induction of Optical Magnetism. *Nano Lett.* **2017**, *17*, 7196−7206.
(46) Banzer, P.; Peschel, U.; Quabis, S.; Leuchs, G. On the Experimental Investigation of the Electric and Magnetic Response of a Single Nano-Structure. *Opt. Express* **2010**, *18*, 10905−10923.
(47) Miroshnichenko, A. E.; Luk'yanchuk, B.; Maier, S. A.; Kivshar, Y. S. Optically Induced Interaction of Magnetic Moments in Hybrid Metamaterials. *ACS Nano* **2012**, *6*, 837−842.
(48) Coenen, T.; Van De Groep, J.; Polman, A. Resonant Modes of Single Silicon Nanocavities Excited by Electron Irradiation. *ACS Nano* **2013**, *7*, 1689−1698.
(49) Wang, L.; Rho, Y.; Shou, W.; Hong, S.; Kato, K.; Eliceiri, M.; Shi, M.; Grigoropoulos, C. P.; Pan, H.; Carraro, C.; Qi, D. Programming Nanoparticles in Multiscale: Optically Modulated Assembly and Phase Switching of Silicon Nanoparticle Array. *ACS Nano* **2018**, *12*, 2231−2241.
(50) Hulst, H. C.; van de Hulst, H. C. *Light Scattering by Small Particles*; Courier Corporation: Chelmsford, MA, 1957.
(51) Kerker, M. *The Scattering of Light and Other Electromagnetic Radiation*; Academic Press: New York, 2016.
(52) Bohren, C. F.; Huffman, D. R. *Absorption and Scattering of Light by Small Particles*; John Wiley & Sons: New York, 2008.
(53) Guclu, C.; Veysi, M.; Darvishzadeh-Varcheie, M.; Capolino, F. Artificial Magnetism *via* Nanoantennas under Azimuthally Polarized Vector Beam Illumination. In *CLEO: Applications and Technology*; Optical Society of America: San Jose, CA, 2016; pp 1−2. DOI: 10.1364/CLEO_AT.2016.JW2A.21.
(54) Guclu, C.; Tamma, V. A.; Wickramasinghe, H. K.; Capolino, F. Photoinduced Magnetic Force between Nanostructures. *Phys. Rev. B: Condens. Matter Mater. Phys.* **2015**, *92*, 235111.
(55) Guclu, C.; Veysi, M.; Capolino, F. Photoinduced Magnetic Nanoprobe Excited by an Azimuthally Polarized Vector Beam. *ACS Photonics* **2016**, *3*, 2049−2058.
(56) Veysi, M.; Guclu, C.; Capolino, F. Vortex Beams with Strong Longitudinally Polarized Magnetic Field and Their Generation by Using Metasurfaces. *J. Opt. Soc. Am. B* **2015**, *32*, 345−354.
(57) Veysi, M.; Guclu, C.; Capolino, F. Focused Azimuthally Polarized Vector Beam and Spatial Magnetic Resolution below the Diffraction Limit. *J. Opt. Soc. Am. B* **2016**, *33*, 2265−2277.
(58) Zhan, Q. Cylindrical Vector Beams: From Mathematical Concepts to Applications. *Adv. Opt. Photonics* **2009**, *1*, 1−57.
(59) Neugebauer, M.; Eismann, J. S.; Bauer, T.; Banzer, P. Magnetic and Electric Transverse Spin Density of Spatially Confined Light. *Phys. Rev. X* **2018**, *8*, 021042.
(60) Fang, X.; Tseng, M. L.; Tsai, D. P.; Zheludev, N. I. Coherent Excitation-Selective Spectroscopy of Multipole Resonances. *Phys. Rev. Appl.* **2016**, *5*, 014010.
(61) Kihm, H. W.; Kim, J.; Koo, S.; Ahn, J.; Ahn, K.; Lee, K.; Park, N.; Kim, D.-S. Optical Magnetic Field Mapping Using a Subwavelength Aperture. *Opt. Express* **2013**, *21*, 5625−5633.
(62) Singh, D. K.; Ahn, J. S.; Koo, S.; Kang, T.; Kim, J.; Lee, S.; Park, N.; Kim, D.-S. Selective Electric and Magnetic Sensitivity of Aperture Probes. *Opt. Express* **2015**, *23*, 20820−20828.
(63) Albooyeh, M.; Simovski, C. R. Substrate-Induced Bianisotropy in Plasmonic Grids. *J. Opt.* **2011**, *13*, 105102.
(64) Albooyeh, M.; Alaee, R.; Rockstuhl, C.; Simovski, C. Revisiting Substrate-Induced Bianisotropy in Metasurfaces. *Phys. Rev. B: Condens. Matter Mater. Phys.* **2015**, *91*, 195304.
(65) Powell, D. A.; Kivshar, Y. S. Substrate-Induced Bianisotropy in Metamaterials. *Appl. Phys. Lett.* **2010**, *97*, 091106.
(66) Miroshnichenko, A. E.; Evlyukhin, A. B.; Kivshar, Y. S.; Chichkov, B. N. Substrate-Induced Resonant Magnetoelectric Effects for Dielectric Nanoparticles. *ACS Photonics* **2015**, *2*, 1423−1428.
(67) Stalder, M.; Schadt, M. Linearly Polarized Light with Axial Symmetry Generated by Liquid-Crystal Polarization Converters. *Opt. Lett.* **1996**, *21*, 1948−1950.
(68) Debus, C.; Lieb, M. A.; Drechsler, A.; Meixner, A. J. Probing Highly Confined Optical Fields in the Focal Region of a High NA Parabolic Mirror with Subwavelength Spatial Resolution. *J. Microsc.* **2003**, *210*, 203−208.
(69) Lerman, G. M.; Yanai, A.; Levy, U. Demonstration of Nanofocusing by the Use of Plasmonic Lens Illuminated with Radially Polarized Light. *Nano Lett.* **2009**, *9*, 2139−2143.
(70) Seo, M. A.; Adam, A. J. L.; Kang, J. H.; Lee, J. W.; Jeoung, S. C.; Park, Q. H.; Planken, P. C. M.; Kim, D. S. Fourier-Transform Terahertz near-Field Imaging of One-Dimensional Slit Arrays: Mapping of Electric-Field-, Magnetic-Field-, and Poynting Vectors. *Opt. Express* **2007**, *15*, 11781−11789.
(71) Woollam, J. A.; McGaham, W. A.; Johs, B. Spectroscopic Ellipsometry Studies of Indium Tin Oxide and Other Flat Panel Display Multilayer Materials. *Thin Solid Films* **1994**, *241*, 44−46.
(72) Kwon, D.-H.; Werner, D. H.; Kildishev, A. V.; Shalaev, V. M. Material Parameter Retrieval Procedure for General Bi-Isotropic Metamaterials and Its Application to Optical Chiral Negative-Index Metamaterial Design. *Opt. Express* **2008**, *16*, 11822−11829.

DOI: 10.1021/acsnano.8b05778
ACS Nano 2018, 12, 12159−12168